Experimental Investigation of Wing Flexibility on Force Generation of a Hovering Flapping Wing Micro Air Vehicle with Double Wing Clap-and-Fling Effects

Q.V. Nguyen*, W.L. Chan, and M. Debiasi
National University of Singapore, 5A Engineering Drive 1, Singapore 117411, Singapore

ABSTRACT

Experimental investigation of wing flexibility on vertical thrust generation and power consumption of a hovering flapping wing micro air vehicle (FW-MAV), namely FlowerFly, weighing 14.5 g with a 3 g onboard battery and having four wings with double wing clap-and-fling effects in hovering condition, was conducted for several wing configurations with the same shape, area, and weight. A data acquisition system was setup to simultaneously record forces, power consumption, and wing motions at various flapping frequencies. The forces and power consumption were measured with a loadcell and a custom-made shunt circuit, respectively, and the wing motion was captured by a high-speed camera. The results show a phase delay of the wing tip displacement observed for wings with high flexible leading edge at high frequency, resulting in less vertical thrust produced when compared with the wings with less leading edge flexibility at the same frequency. Positive wing camber was observed during wing flapping by arranging the wing supporting ribs. Comparison of thrust-to-power ratio between the wing configurations was undertaken to figure out a wing configuration for high vertical thrust production but less power consumption.

1 INTRODUCTION

Vertical Takeoff and Landing (VTOL), agile maneuvering, and hovering flight are extremely desirable features of flying insects in development of Flapping-Wing Micro Air Vehicles (FW-MAVs), which enable an insect-inspired FW-MAV to retake off and fly in confined spaces for indoor surveillance. Moreover, FW-MAVs have been proven to be more efficient at low Reynolds number regime (typically from 10^3 to 10^5 [1]) under unsteady aerodynamics when their size becomes less than 15 cm. This is because FW-MAVs benefit from unsteady aerodynamic mechanisms at low Reynolds number: wing leading vortex and delayed stall [2], wing clap-and-fling [3], and wing rotation and wake capture [4, 5]. Operation-wise, FW-MAVs flap their wings at relatively low frequencies and fly at low forward speed or hovering, resulting in producing less noise, and less dangerous than their counter parts of fixed wings flying at high forward speed and rotary wings operating at high motor or propeller speed. However, the payload ability of FW-MAVs is very limited in sub-10 g due to their nature of small size and light weight. Therefore, there are a number of experimental reports looking into changing the wing designs of various FW-MAVs, such as changing materials of wing membrane, wing aspect ratio, wing supporting veins for aerodynamic force enhancement [6, 7, 8]. However, and the wing mass was not kept the same for all cases of wing configurations.

Figure 1: The FlowerFly with onboard camera and control system for pitch-, yaw-, and roll-control controlled by three servos.

As a continuing effort to increase the payload ability for our FlowerFly [9], see Figure 1, for more system integration on the next version, we have improved the aerodynamic force generation ability of the FlowerFly by experimentally inves-

*Email address(es): tslnqv@nus.edu.sg

tigating various wing configurations with different flexibility in both spanwise and chordwise. The aim is to find a set of wings that can generate high vertical thrust, but consumes low power. In order to avoid effect of wing shape, wing aspect ratio, and wing inertia difference between wing configurations, the wing shape, area, and wing mass are kept the same for all cases. Experimental investigation was conducted for five different wing configurations to acquire vertical thrusts, power consumptions, and flapping wing motions. All acquired data was synchronized with a trigger. Wing efficiency was characterized by thrust-to-power ratio, which is defined as the ratio of the vertical thrust to the input power or power consumption. In addition, the design of gearbox using one motor to simultaneously drive four wings and create double wing clap-and-fling is also described.

2 Materials and Methods

2.1 *Flapping mechanism and gearbox*

Flapping mechanism is one of the challenging parts in the design. It converts the rotary motion of the motor or crank into flapping motion of wings. In this design, we used a combination of crank-slider mechanism and linkage mechanism, see Figure 2. The rotary motion of the crank is transformed into the linear motion of the slider engaging in the slot through the connecting link, and then the linear motion of the slider is transformed into the flapping motion of the coupler to where the wings are attached.

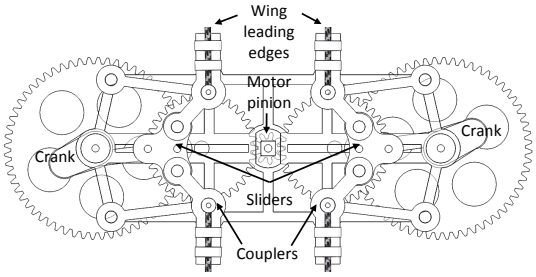

Figure 2: Gearbox with double clap-and-fling mechanisms.

Figure 3 shows a comparison between a sinusoidal function and wing flapping angle produced by the designed gearbox for one flapping cycle. The flapping angle is close to the sinusoidal function; that help to avoid high angular acceleration or wing inertia during flapping. We have invented a gearbox with a gear ratio of 1 to 20 [9] to synchronously drive four wings and create double wing clap-and-fling effects during one flapping cycle. The gearbox combines two modules driven by a brushless motor (AP02, Kv = 7000, hobbyking.com) controlled by an electronic speed controller (Mi-3A ESC module, hobbyking.com), see Figure 2. Each module consists of a crank-slider and linkage (two couplers and two output links). There are wing holders installed on the coupler for wing attachment. The flapping angle of each coupler or wing is designed to be 90^o, correspondingly, the four

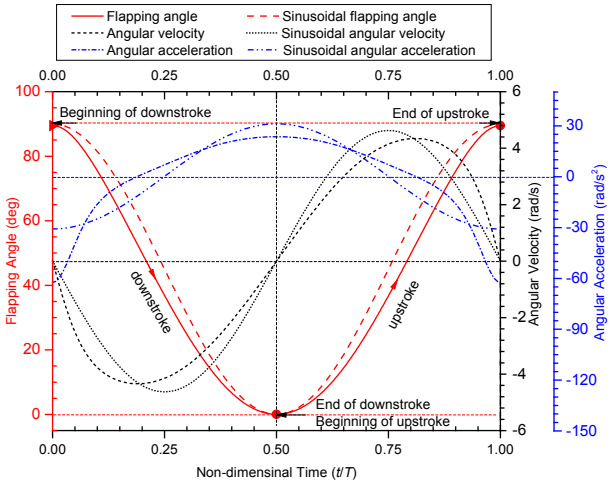

Figure 3: Flapping angles, angular velocities, and angular accelerations of the flapping mechanism (red line for flapping angle, black line for angular velocity, and blue line for angular acceleration. The sinusoidal functions are only for reference.)

wings sweep a flapping angle of 360^o for a flapping cycle. The double wing clap-and-fling effects, see Figure 4, can be created at the end of each half flapping stroke: downstroke and upstroke. The large flapping angle and wing clap-and-fling effects are expected to produce high thrust.

2.2 *Wings*

We use lightweight materials such as thin carbon rod (0.6 mm rod and 0.7 mm tube for leading edge and 0.3 - 0.5 mm rods for wing ribs or supporting veins) and thin Mylar film (5 μm) for wing fabrication. The detail fabrication process can be found in reference [10]. In order to investigate the effect of wing flexibility on vertical thrust and power consumption while avoiding wing inertia difference between the wings, various wings with the same shape, area, wing membrane thickness (5 μm Mylar film), and weight, but different wing leading edge diameters (0.6 mm carbon rod, and 0.7 mm carbon tube) and supporting veins (0.5 mm and 0.3 mm carbon rods) were fabricated and used, see Table 1. The wing *AR* of an individual wing is 1.68; the wing length (root to tip) was 110 mm, with maximum and mean chord lengths of 66.7 mm and 65.3 mm, respectively, and the surface area of each wing is 7184 mm^2. Weight difference between these wings is only 3.6%, thus the effect of wing inertia difference between the wings can be assumed the same for all wings and neglected in comparison between these wings even though the wing mass distribution along the wing span is slightly different. Figure 5 shows the wing design for five cases. The wings can be divided into two wing groups; Group#1 includes Wing#1 and Wing#2 with the same leading edge stiffness (0.6 mm carbon rod) and slight difference in chordwise stiffness, see Figure 5, and Group#2 includes Wing#3, Wing#4, and Wing#5 with

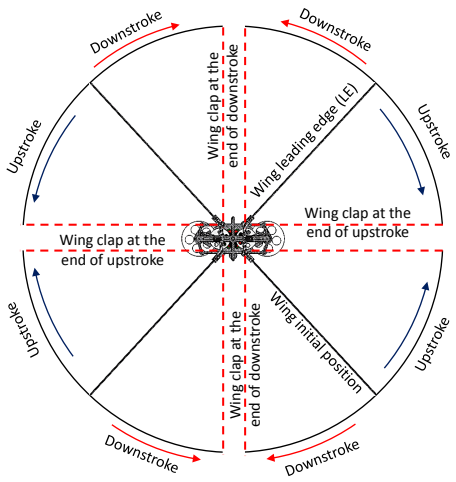

Figure 4: Flapping strokes of the gearbox and double wing clap-and-fling at the end of downstroke and upstroke.

the same leading edge stiffness (0.7 mm carbon tube) and different chordwise stiffness.

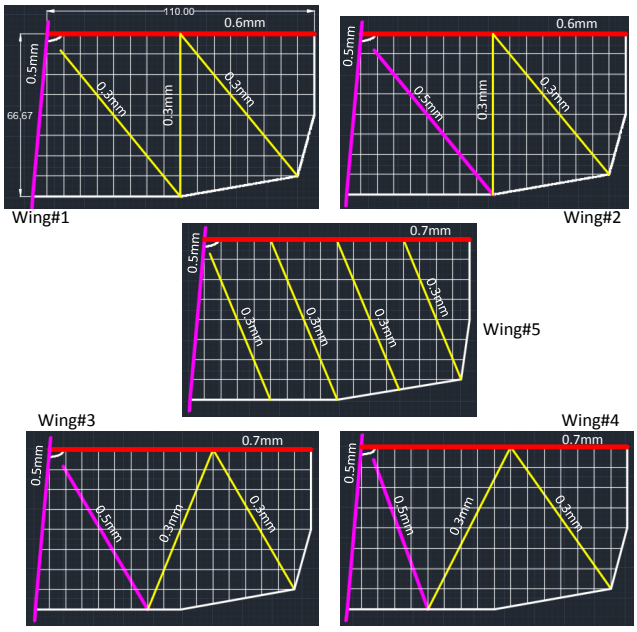

Figure 5: Fabricated wings made of Mylar film and carbon rods.

2.3 *Experimental apparatus*

The experimental apparatus consists of the FW-MAV, FlowerFly, without tail equipped with a Neodymium magnet placed in the gearbox, a radio receiver (DTRx31d, 2.4 GHz, Deltang, UK), and controlled by a transmitter (DX7, 2.4 GHz DSM2, Spektrum, USA), a test jig for mounting the FW-MAV, a 3-axis force/torque loadcell (Nano 17 Titanium, ATI Industrial Automation, USA) for force measurement, a

#	Leading edge (mm)	N. of veins	Span (mm)	Area (mm^2)	Mass (g) (difference)
1	0.6	3	110	7184	0.28*
2	0.6	3	110	7184	0.29 (3.6%)
3	0.7	3	110	7184	0.29 (3.6%)
4	0.7	3	110	7184	0.29 (3.6%)
5	0.7	4	110	7184	0.28*

Table 1: Parameters of wings, *mass reference.

custom-made shunt circuit for current and voltage measurement and a tachometer built in house with Hall Effect sensor for frequency readings, a high speed camera (Phantom Miro M320S, LaVision, Germany) for flapping wing motion capture, a power supply (Tenma 72-8350, China), a data acquisition card (DAQ card BNC-2110, National Instrument, USA) for acquiring data, a PC for data reading and recording, and an in-house built trigger for data synchronization. The experimental setup was shown in Figure 6.

2.4 *Measurement of force, power, and wing motion*

All the flapping tests were conducted in still air in hovering condition from 9 Hz onward the maximum frequency that the FW-MAV can operate at full throttle level. Lower frequencies than 9 Hz were refrained from experiment due to low force expected. Data acquisition for each wing configuration was repeated five times for each flapping frequency. Since the two pairs of wings flap symmetrically in opposite phase, see Figure 4, the forces in horizontal plane or horizontal forces acting on each wing are canceled by each other. Thus, only force in vertical direction or vertical thrust can be acquired by the loadcell.

The FW-MAV was directly mounted to the loadcell, and then firmly installed into the test jig in vertical configuration; this is similar to the free hovering flight condition of the FlowerFly. The power supply maintained the applied voltage of 3.7 V (equivalent to a single cell LiPo battery) to the motor. The transmitter generated the PWM (Pulse Width Modulation) command and transmitted it to the receiver for controlling the motor speed or flapping frequency of the FW-MAV through the ESC. The flapping frequency acquired by the Hall Effect sensor and tachometer was sent to the PC for readings. Data of force, power in terms of voltage and current, and high speed images of wing motion were acquired at the same time with the trigger. When the trigger was turned on the Hall Effect sensor picked up the magnetic signal from the Neodymium magnet and transmitted an electrical pulse to simultaneously activate the high speed camera, the loadcell, and the shunt circuit for data recording. Thus, the images recorded from the camera were synchronized with the data of

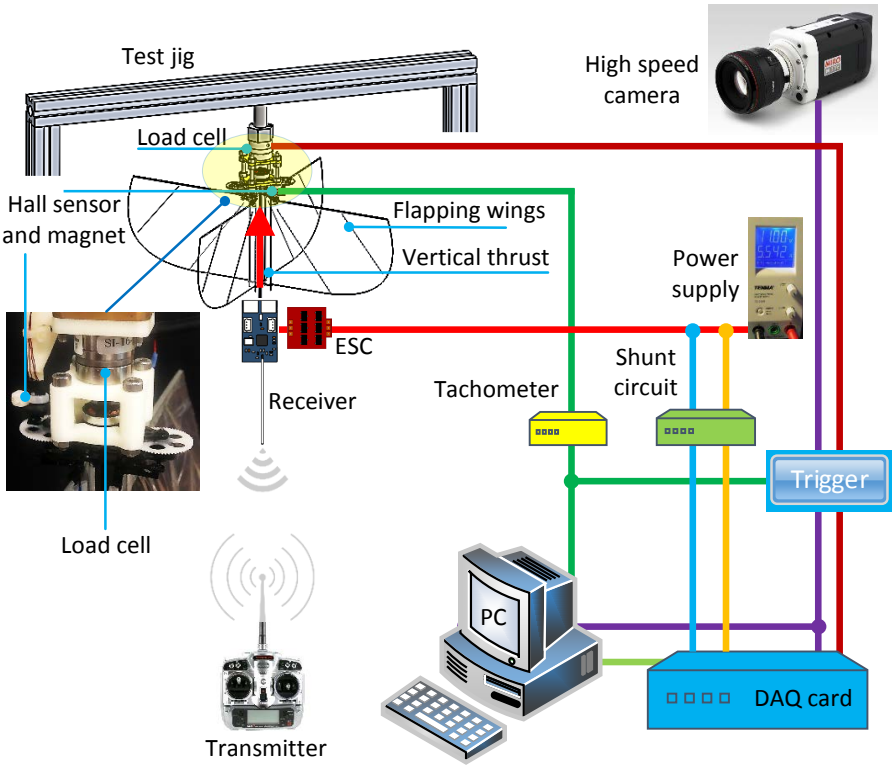

Figure 6: Experimental apparatus and set-up for measurement and synchronization of forces, power, and wing motion.

force and power consumption. The sampling rate of force, power, and wing motion was set at the same frequency of 5 kHz to avoid time shift of the recorded data.

2.5 Data process

Contaminated noise due the vibration of the flapping-wing system and structural vibration of the test jig was filtered out by a low pass filter with a cut-off frequency of 3 times greater than the flapping frequency as recommended by the reference [11]. 20 flapping cycles was taken from each measurement (out of five), and then averaged to represent the cycle-averaged value of each measurement. Afterward, we calculated the statistical mean value of five cycle-averaged values to represent the cycle-averaged force and power consumption of the FW-MAV. The high speed images of wing motion were used to examine the wing deformation in terms of spanwise and chordwise deformation as well as interpret the vertical force and power consumption histories.

3 Result and Discussions

3.1 Time-dependent vertical thrust

The typical instantaneous vertical thrust, power consumption, and flapping angle synchronized with each other are plotted in Figure 7 with respect to (w.r.t) non-dimensional time for one flapping cycle. The instantaneous vertical thrust displays two peaks with different magnitude and two troughs with almost the same magnitude of nearly zero. From the high speed camera images, the first peak and second peak are found to occur at the end of wing fling during downstroke and upstroke, respectively, while the effects of wing clap are not clearly seen. This phenomenon is due to the passive wing rotation mechanism used in the FW-MAV [9], the wings cannot actively rotate to push the air down when the two wing leading edge approach each other. The two troughs are almost zero and found to occur at the beginning of downstroke and upstroke, respectively, where the wings are almost aligned in vertical direction, i.e., angle of attack of the flapping wing is almost 90^0. Similarly, the power consumption history also displays two peaks and two troughs in one flapping cycle with slightly phase shift compared to the vertical thrust history at the first peak and second peak, respectively. It also can be seen that the FW-MAV produces asymmetrical vertical thrust peaks during downstroke and upstroke. The thrust peak at the end of wing fling during upstroke is higher than that at the end of wing fling during downstroke. This phenomenon is due to the wing root gap difference in the gearbox design and slightly tolerance of the gearbox assembly, resulting in wing clap-and-fling more fully at the end of upstroke than downstroke.

Figures 8 - 12 show the vertical thrust history synchronized with power consumption for one flapping cycle. The positive values dominate the force profiles in both half flap-

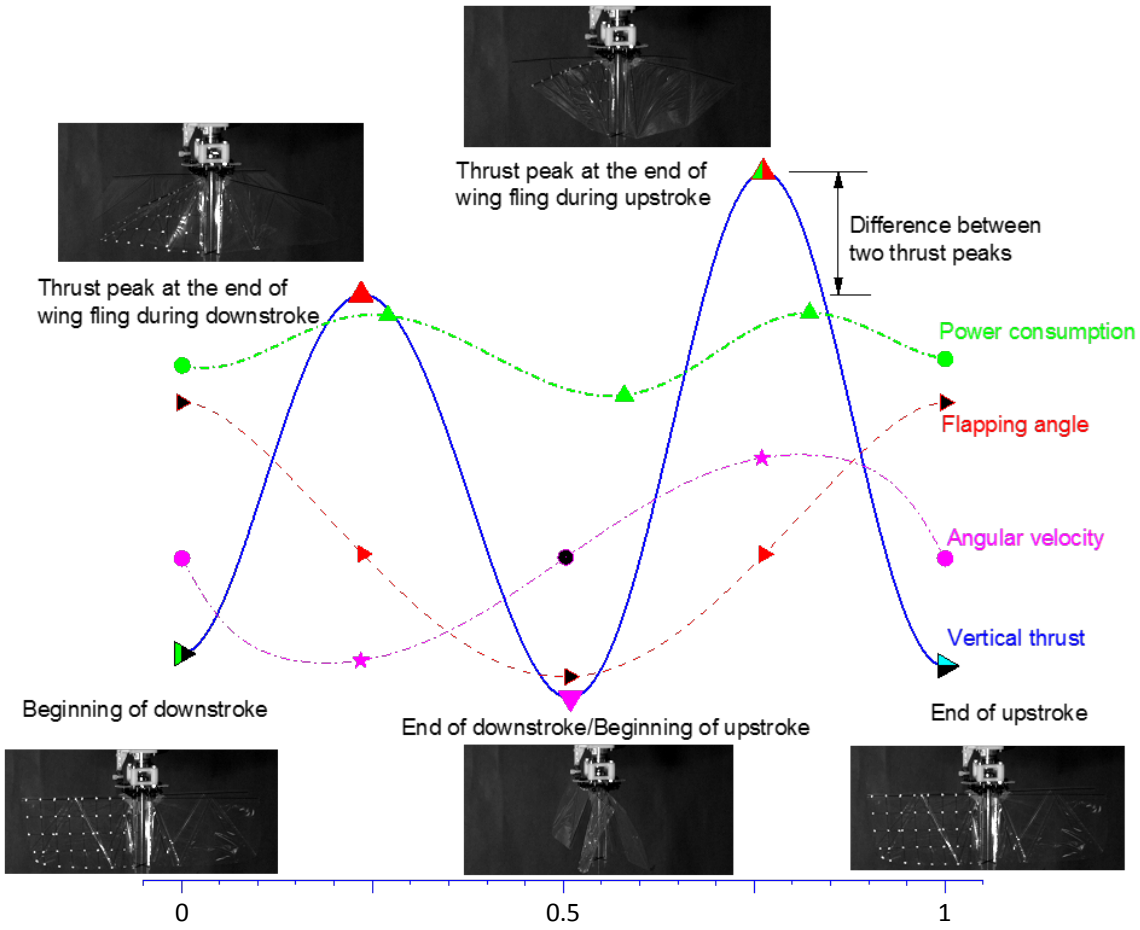

Figure 7: Typical vertical thrust and power consumption histories of the FW-MAV for one flapping cycle; flapping angle and angular velocity are for reference.

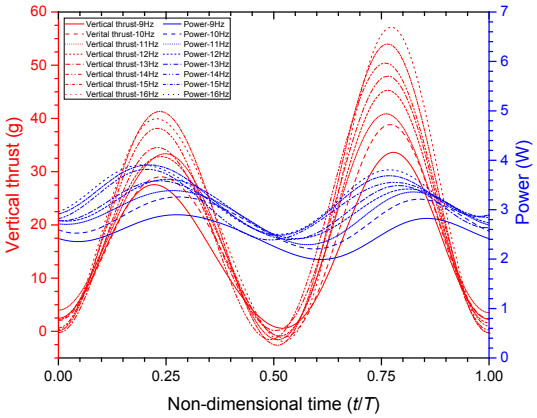

Figure 8: Time-dependent vertical thrust of Wing#1 for various frequencies .

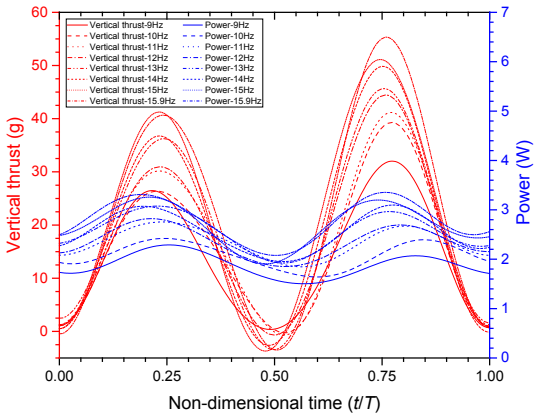

Figure 9: Time-dependent vertical thrust of Wing#2 for various frequencies.

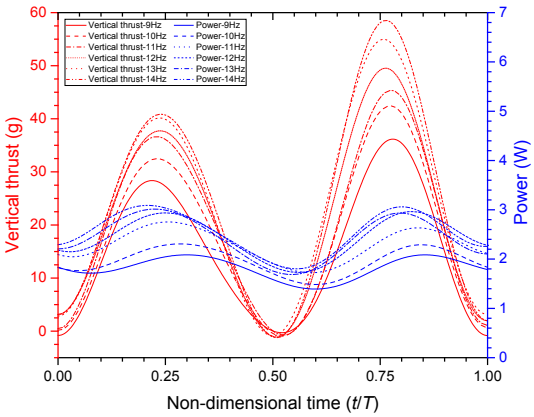

Figure 10: Time-dependent vertical thrust of Wing#3 for various frequencies.

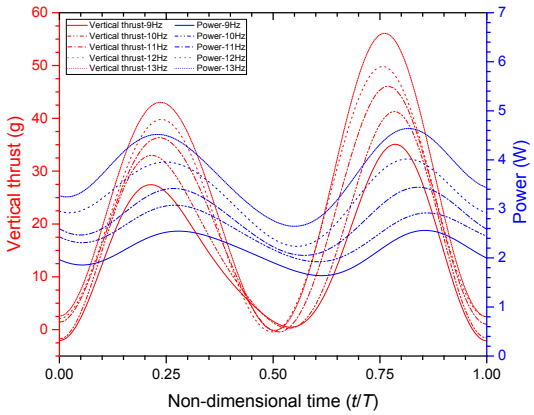

Figure 11: Time-dependent vertical thrust of Wing#4 for various frequencies.

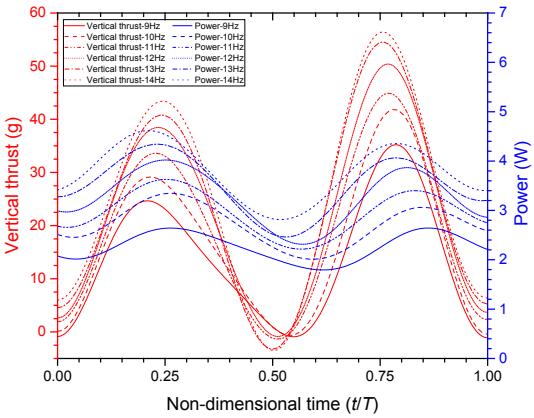

Figure 12: Time-dependent vertical thrust of Wing#5 for various frequencies.

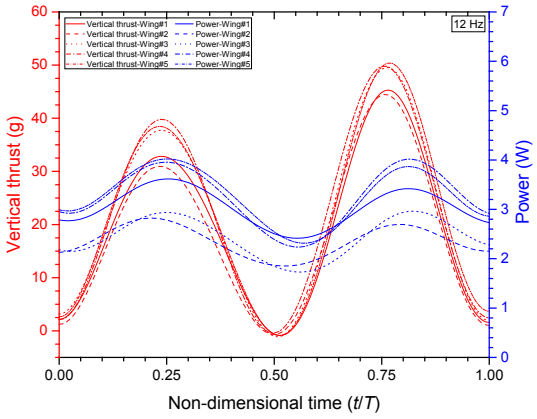

Figure 13: Vertical thrust and power consumption of five wing configurations at flapping frequency of 12 Hz for one flapping cycle.

ping strokes: downstroke and upstroke, resulting in positive cycle-averaged vertical thrust. The results indicate that the flapping frequency significantly influences the vertical force and power consumption. Higher flapping frequency yields a considerable increase in vertical thrust history at the region around the two peaks while the two troughs are almost not affected, and remain at nearly zero. Power consumption is shifted up in similar patterns as flapping frequency increases.

Figure 13 shows comparisons of vertical thrusts and power consumption of five wing configurations at flapping frequency of 12 Hz for one flapping cycle. It can be seen that the wings with more rigid leading edge (Group#1, 0.7 mm carbon tube leading edge) significantly increase the two vertical thrust peaks when compared with the wings with less rigid leading edge (Group#2, 0.6 mm carbon rod leading edge). The two troughs in the vertical thrust are not affected by the wing spanwise flexibility in both Group#1 and #2, and remain the same value at nearly zero. In general, the wings with the same wing leading edge stiffness (0.7 mm carbon tube, 0.6 mm carbon rod) produce similar vertical thrust history; only slightly difference was observed, see Figure 13. It is suggested that the wing leading edge stiffness plays more important role in vertical thrust production than the wing chordwise flexibility.

3.2 Maximum flapping frequency and vertical thrust

Given the same motor and gearbox, the maximum flapping frequency of the FW-MAV is depended on not only wing mass or inertia but also wing frontal area which is determined by the wing area projected on the plane perpendicular to the wing motion direction. Larger frontal wing area is subjected to more drag, and vice versa. When the wing configurations are changed, the wing deformation as well as wing rotation angle are passively changed. The wing deformation in spanwise and chordwise as well as wing rotation change the frontal area of the flapping wing, resulting in change of

drag acting on the wing. Thus, different wing configuration has different flapping frequency at a given throttle level. Figure 14 shows maximum flapping frequency and vertical thrust of five wing configurations at maximum throttle level. The results indicate that the wings in each group (Group#1 and Group#2) show similar maximum frequency and vertical thrust. Moreover, it was observed from the high speed images of wing motion that the wings in Group#1 (Wing#1 and Wing#2) have larger wing deformation in spanwise direction than the wings in Group#2 (Wing#3, Wing#4, and Wing#5). Phase delay of wing tip displacement, i.e., the wing tip and wing root move in opposite direction was observed only in the wings in Group#1. Again, based on the results shown in Figure 14 it can be concluded that maximum flapping frequency and vertical thrust mostly depend on wing leading edge stiffness in spanwise direction, slightly change in chordwise stiffness plays marginal role in contribution to the maximum frequency and vertical thrust.

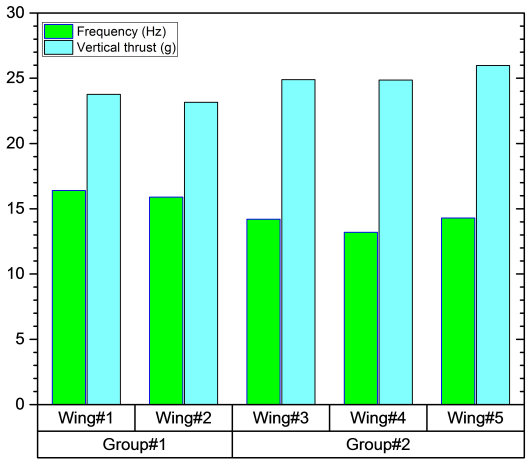

Figure 14: Maximum flapping frequency and vertical thrust of various wing configurations at maximum throttle level.

3.3 Cycle-averaged vertical thrust and power consumption

The results shown in Figure 15 indicate almost a nearly linear relationship between cycle-averaged vertical thrust and flapping frequency for all wing configurations. Theoretically, the vertical thrust or lift is proportional to the velocity or frequency square. Therefore, the nearly linear relationship obtained from the experiment can be explained by the induced velocity which reduces the effective angle of attack on the flapping wing. The induced velocity tends to be increased as the flapping frequency increases, thus, resulting in reducing effective angle of attack on the flapping wing or resulting in reducing vertical thrust on the wing. Again, it can seen the wings with the same leading edge stiffness produce similar cycle-averaged vertical thrust at the same flapping frequency. And the wings with more rigid leading edge generate more vertical thrust than the wing with less rigid leading edge.

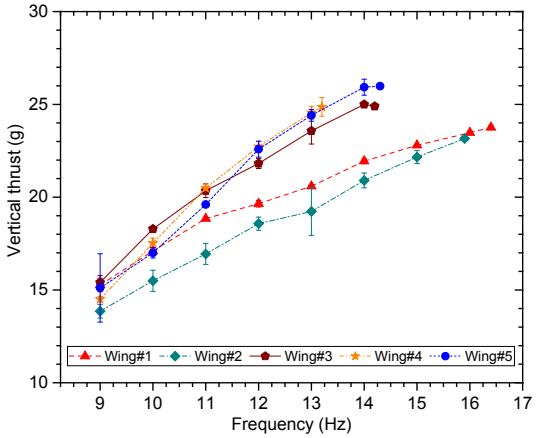

Figure 15: Vertical thrust w.r.t flapping frequency for various wing configurations.

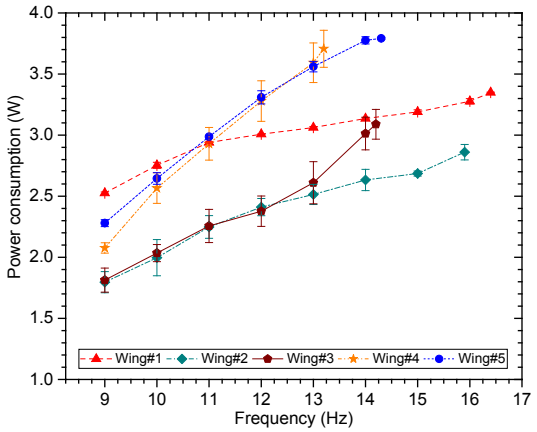

Figure 16: Power consumption w.r.t flapping frequency for the various wing configurations.

The power consumption also increases almost linearly with the flapping frequency. The wings with the same leading edge stiffness show the similar trend in power consumption, see Figure 16. Figure 17 indicates the thrust to power ratio for each wing configuration. This curve is relative flat with respect to frequency; there is about one unit difference from 9 Hz to the maximum flapping frequency of each wing. Wing#3 shows similar cycle-averaged vertical thrust to the Wing#4 and Wing#5 while consuming less power, resulting in the highest thrust to power ratio among the five wings. This is due to the more uniform wing rotation from wing root to wing tip, and positive wing camber created during flapping compared with the other wings, which was observed by the high speed images of wing motion. Wing#1 produces comparable vertical thrust, but consumes more power at frequencies lower than 14 Hz, resulting in inefficiency of thrust-to-power ratio. Overall, it is clear that spanwise wing flexibility influence both the vertical thrust history and power consump-

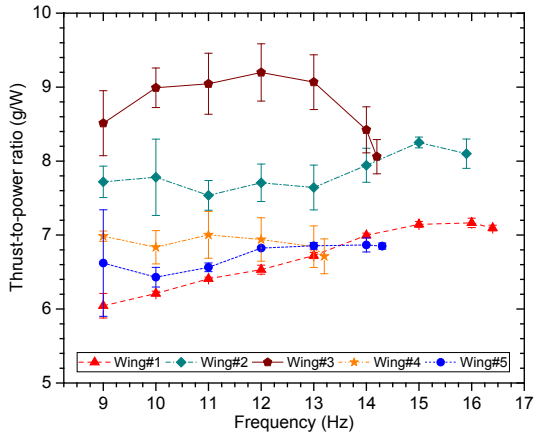

Figure 17: Thrust-to-power ratio w.r.t flapping frequency for the various wing configurations.

tion, while the chordwise wing flexibility plays marginal effect. The wings with the same leading edge stiffness produce similar patterns of both vertical thrust and power consumption histories, and also similar trend in cycle-averaged vertical thrust and power consumption.

4 Conclusion

Experiments have been conducted to investigate the wing flexibility on vertical thrust production and power consumption of a FW-MAV with double wing clap-and-fling effects, namely FlowerFly, which has two pairs of wings and a weight of 14.5 g. In summary, the following conclusions can be derived from this study: 1) Two vertical thrust peaks with different magnitude and two vertical thrust trough with almost zero magnitude were observed within one flapping cycle. Due to the passive wing rotation mechanism used in the FW-MAV, the vertical thrust peaks at about 25% and 75% flapping cycle, respectively, are created by the wing fling rather than the wing clap. The lower and higher peaks occur at the end of wing fling during downstroke and upstroke, respectively. 2) At flapping frequency of 9 Hz, the FlowerFly is about to produce enough vertical thrust for lift-off. Higher flapping frequency produces larger vertical thrust peaks while thrust troughs remain unchanged at almost zero value. 3) Wings with the same leading edge stiffness produce similar vertical thrust history and cycle-averaged vertical thrust. At the same flapping frequency, wings with stiffer leading edge produce higher thrust peaks, resulting in larger averaged thrust compared with the wing with less leading stiffness. Wing chordwise stiffness plays marginal role in both vertical thrust history and cycle-averaged thrust.

References

[1] T. Nakata, H. Liu, Y. Tanaka, N. Nishihashi, X. Wang, and A. Satoi. Aerodynamics of a bioinspired flexible flapping-wing micro air vehicle. *Bioinspiration& Biomimetics*, 6(4):1–11, 2011.

[2] C.P. Ellington, C. Van Den Berg, A.P. Willmott, and A.L.R. Thomasi. Leading-edge vortices in insect flight. *Nature*, 384:626–630, 1996.

[3] T. Weis-Fogh. Unusual mechanisms for the generation of lift in flying animals. *Scientific American*, 233:80–87, 1975.

[4] M.H. Dickinson, F.O. Lehmann, and S.P. Sane. Wing rotation and the aerodynamic basis of insect flight. *Science*, 284:1954–1960, 1999.

[5] S.P. Sane. The aerodynamics of insect flight. *The Journal of Experimental Biology*, 206:4191–4208, 2003.

[6] L. Zhao, Q. Huang, X. Deng, and S.P. Sane. Aerodynamic effects of flexibility in flapping wings. *Journal of The Royal Society Interface*, 7:485–497, 2010.

[7] H. Hua, A.G. Kumar, G. Abate, and R. Albertanic. An experimental investigation on the aerodynamic performances of flexible membrane wings in flapping flight. *Aerospace Science and Technology*, pages 575–586, 2010.

[8] S. Deng, M. Percin, B. van Oudheusden, B. Remes, and H. Bijl. An experimental investigation on the aerodynamic performances of flexible membrane wings in flapping flight. *International Journal of Micro Air Vehicles*, 6(2):105–115, 2014.

[9] Q.V. Nguyen, W.L. Chan, and M. Debiasi. Performance tests of a hovering flapping wing micro air vehicle with double wing clap-and-fling mechanism. In *The International Micro Air Vehicle Conference and Competition*, Aachen, Germany, 2015.

[10] Q.V. Nguyen, W.L. Chan, and M. Debiasi. Hybrid design and performance tests of a hovering insect-inspired flapping-wing micro aerial vehicle. *Journal of Bionic Engineering*, 13:235–248, 2016.

[11] J.V. Caetano, M. Percin, B.W. van Oudheusden, B. Remes, C. de Wagter, G.C.H.E. de Croon, and C.C. de Visser. Error analysis and assessment of unsteady forces acting on a flapping wing micro air vehicle: free flight versus wind-tunnel experimental methods. *Bioinspiration& Biomimetics*, 10:1–21, 2015.